## APPENDIX

## REFERENCES


[1] D. Eberly. *Ridges in Image and Data Analysis*. Kluwer Acadamic Publishers, Dordrecht, 1996.

[2] B. Schindler, R. Peikert, R. Fuchs, and H. Theisel. Ridge Concepts for the Visualization of Lagrangian Coherent Structures. *Proceedings of TopoInVis*, pages 1–14, 2011.

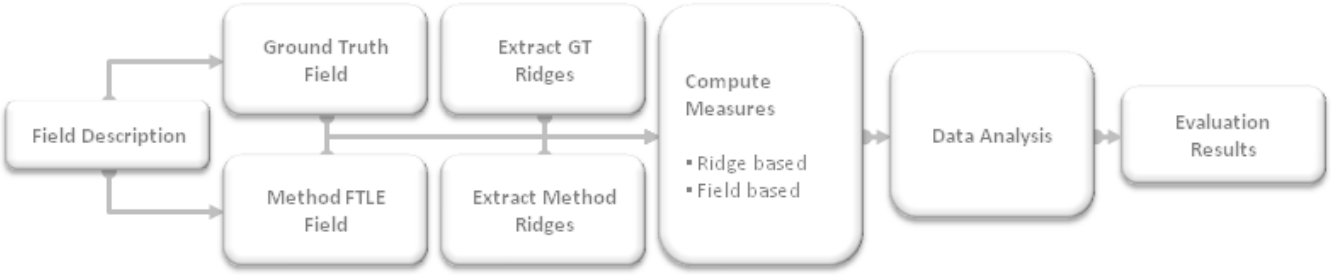


Figure 1: Overview of the proposed benchmarking process and necessary steps in order to compare sets of FTLE fields.

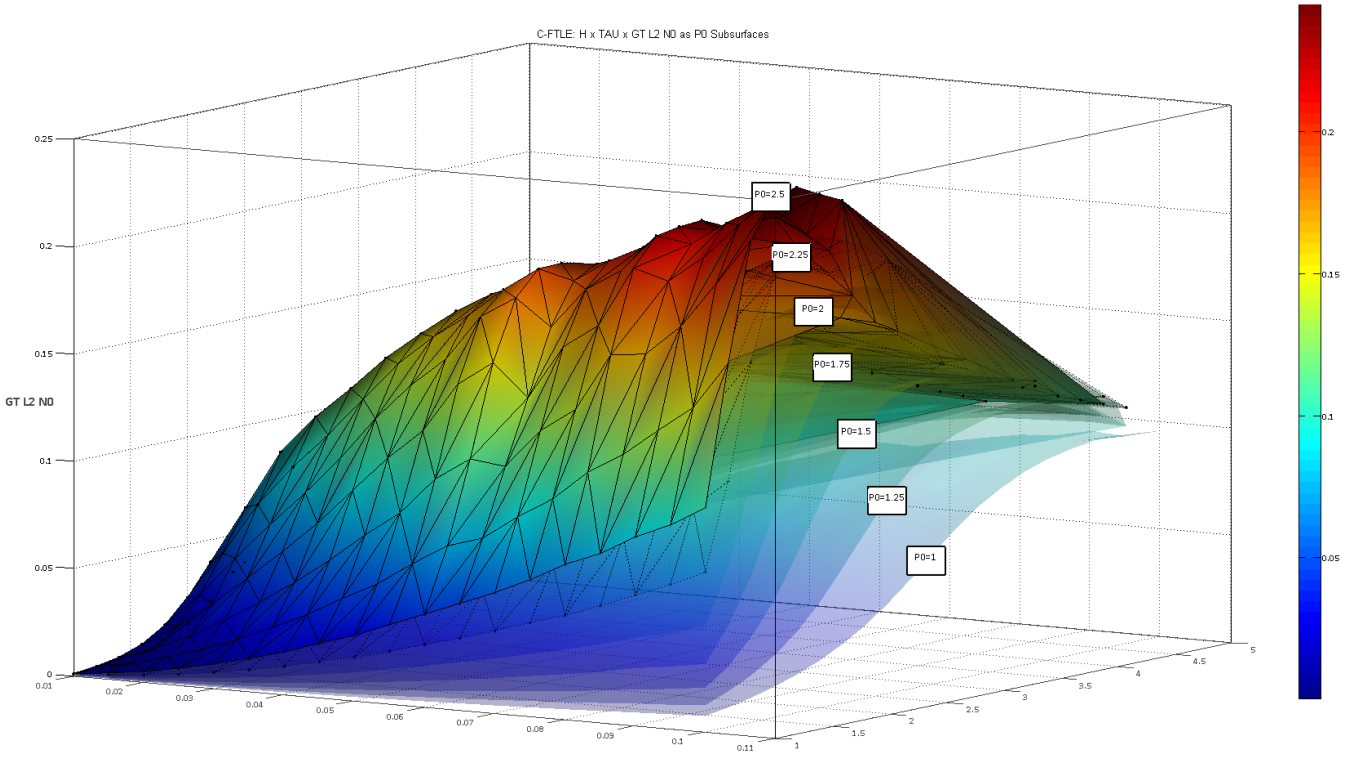


Figure 2: **Sine ridge**: If the sampling subspace integration time $TAU$ versus resolution $H$ against the field based error of the $\ell^2$ norm $GT\_L2\_N0$ is considered, the additional field parameter $P0$ allows to create multiple error surfaces. Plotting them against each other, indicates a linear trend between increasing ridge sharpness and the resulting field error (color coded).

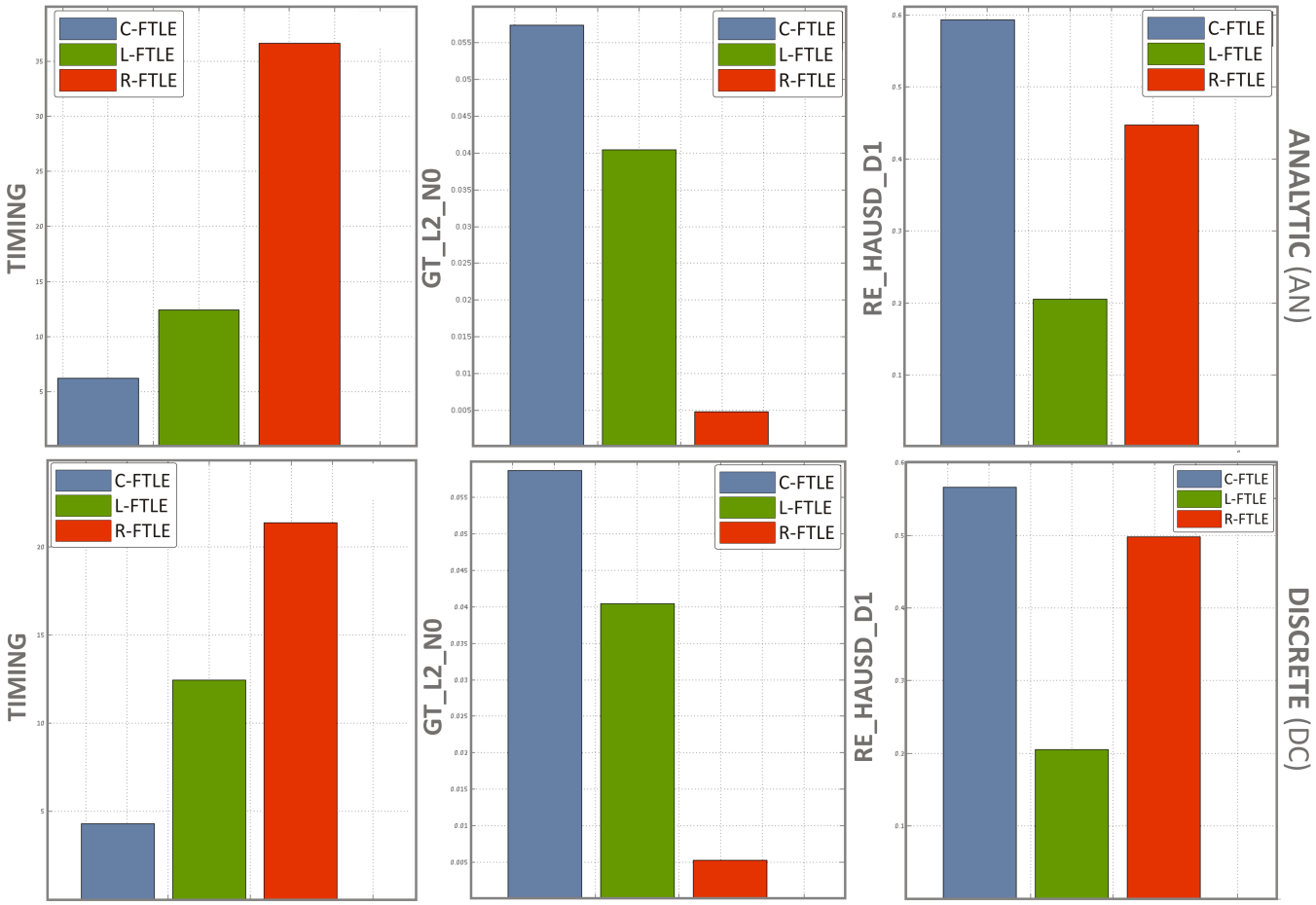


Figure 3: **Sine ridge:** Bar plots showing the averaged results among all measured samples for computation time $TIMING$, FTLE field error $GT\_L2\_N0$ and ridge deviation error $RE\_HAUSD\_D1$.

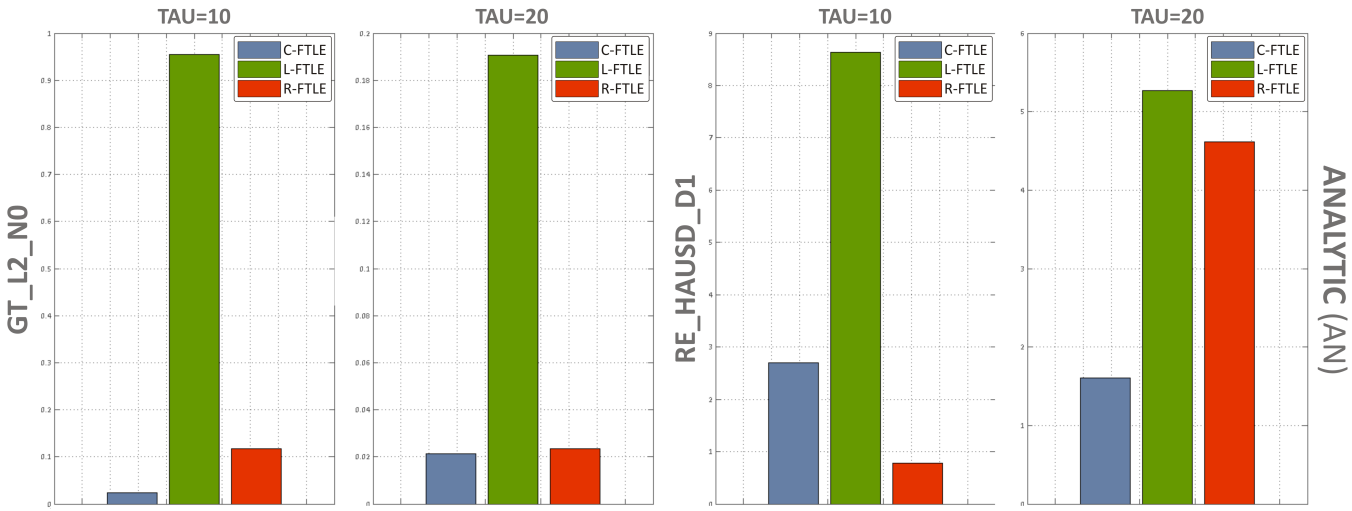


Figure 4: **Spiral focus:** Bar plots showing the averaged results among all analytically computed samples for the field error and ridge error for integration time $TAU = 10$ and $TAU = 20$.

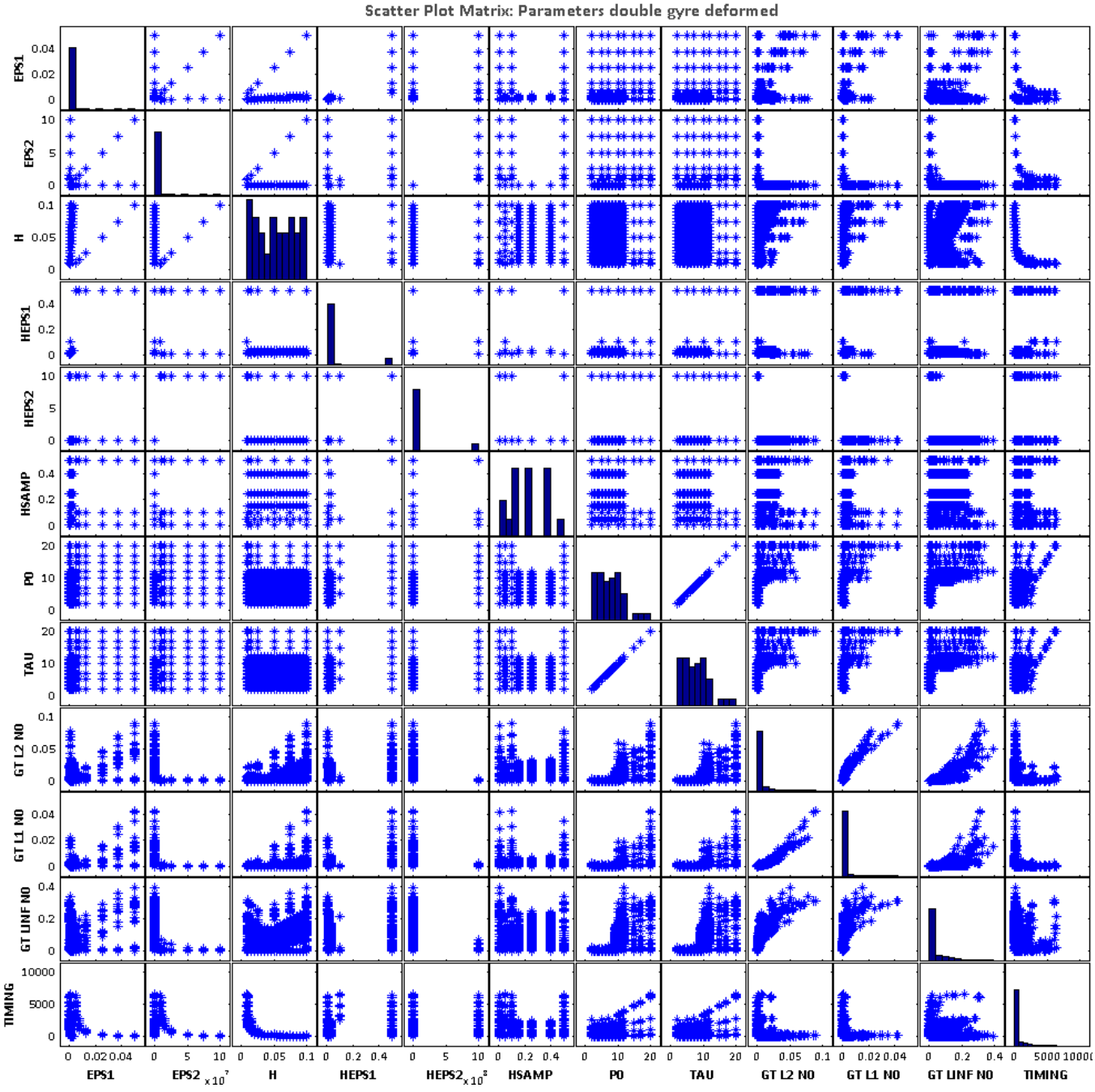


Figure 5: **Double gyre deformed**: Scatter plot for all base parameters and computed samples. Note that every point represents one computed FTLE field.

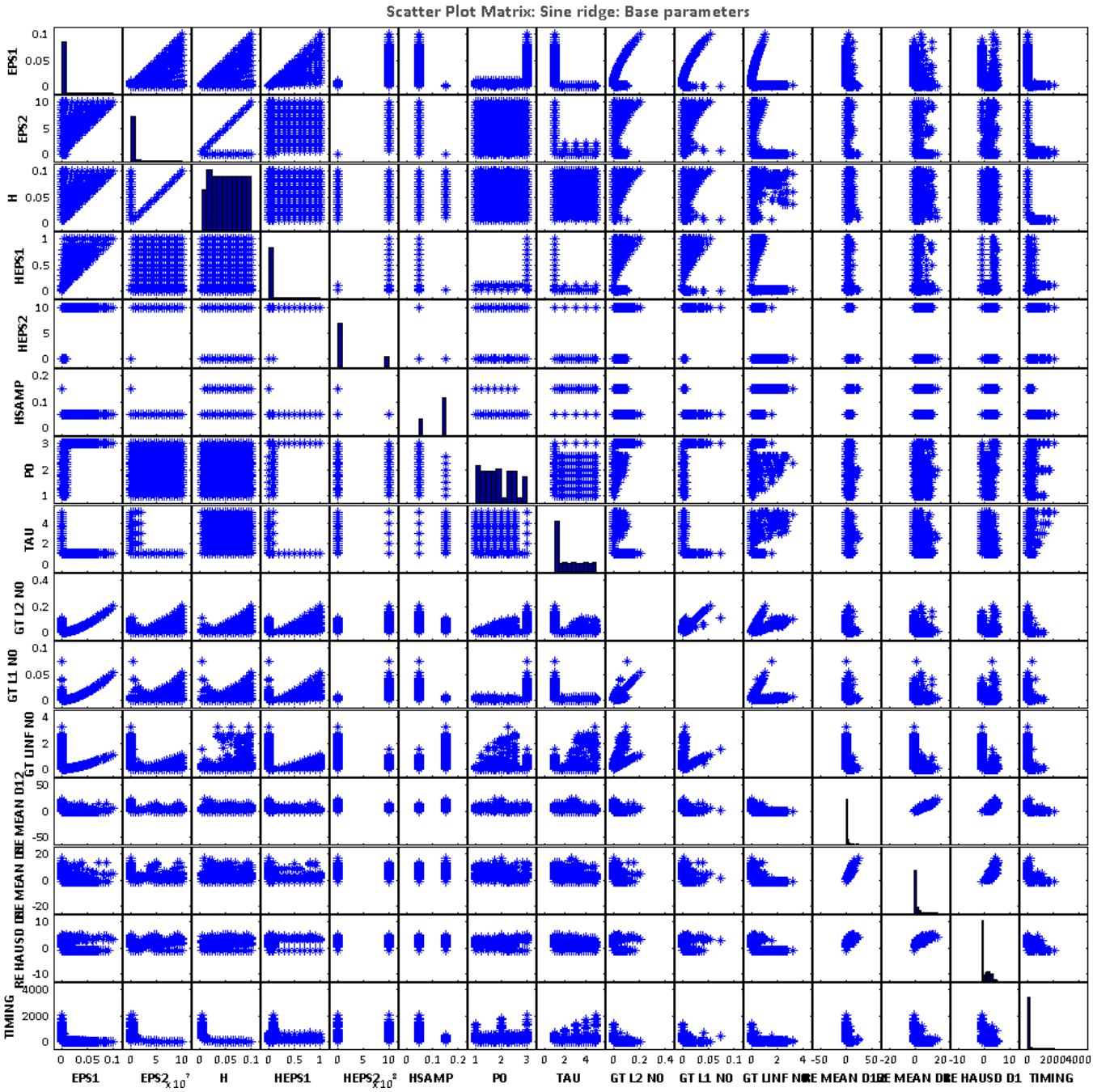


Figure 6: **Sine ridge**: Scatter plot for all base parameters and computed samples. Note that every point represents one computed FTLE field.

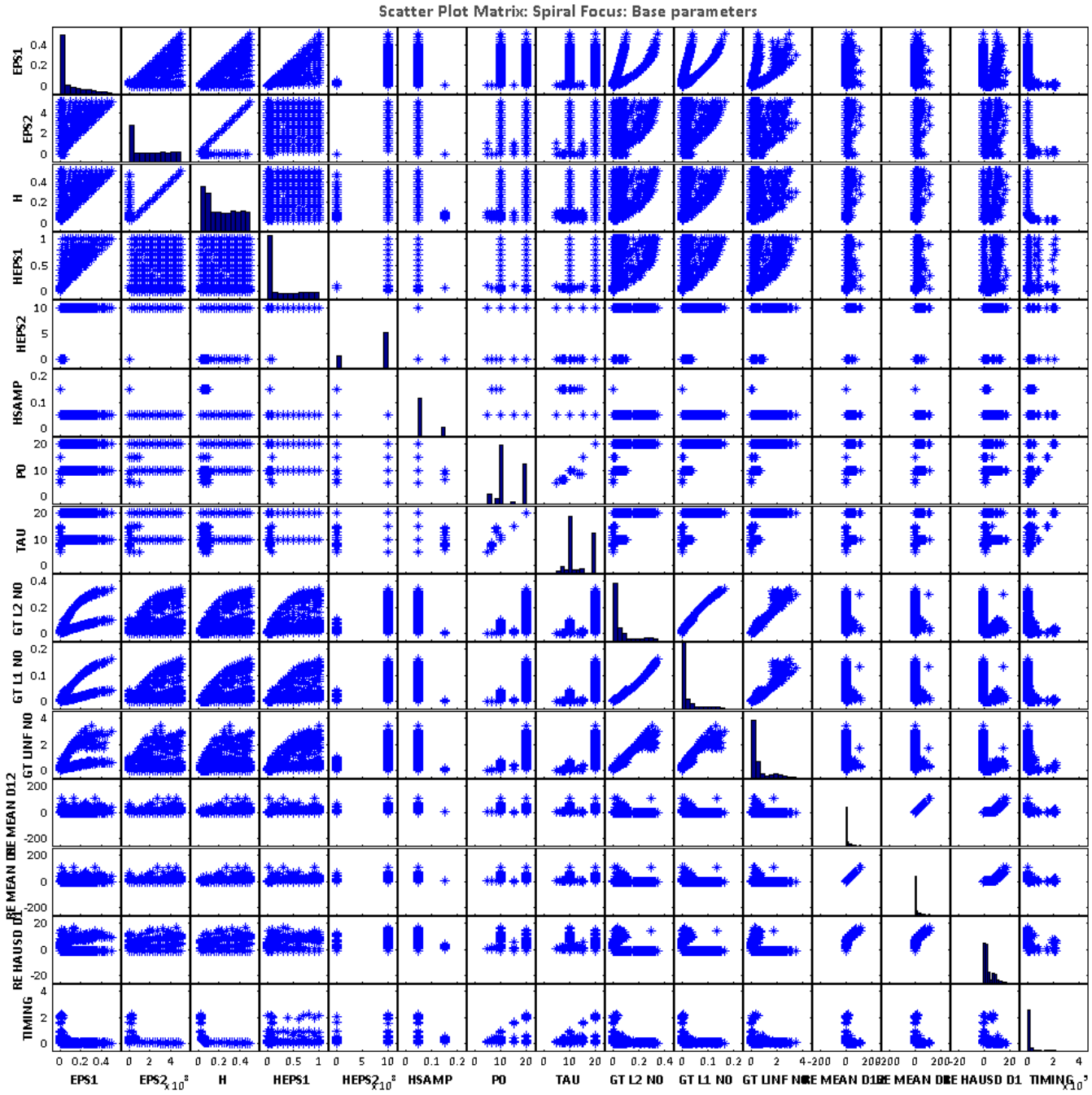


Figure 7: **Spiral focus**: Scatter plot for all base parameters and computed samples. Note that every point represents one computed FTLE field.

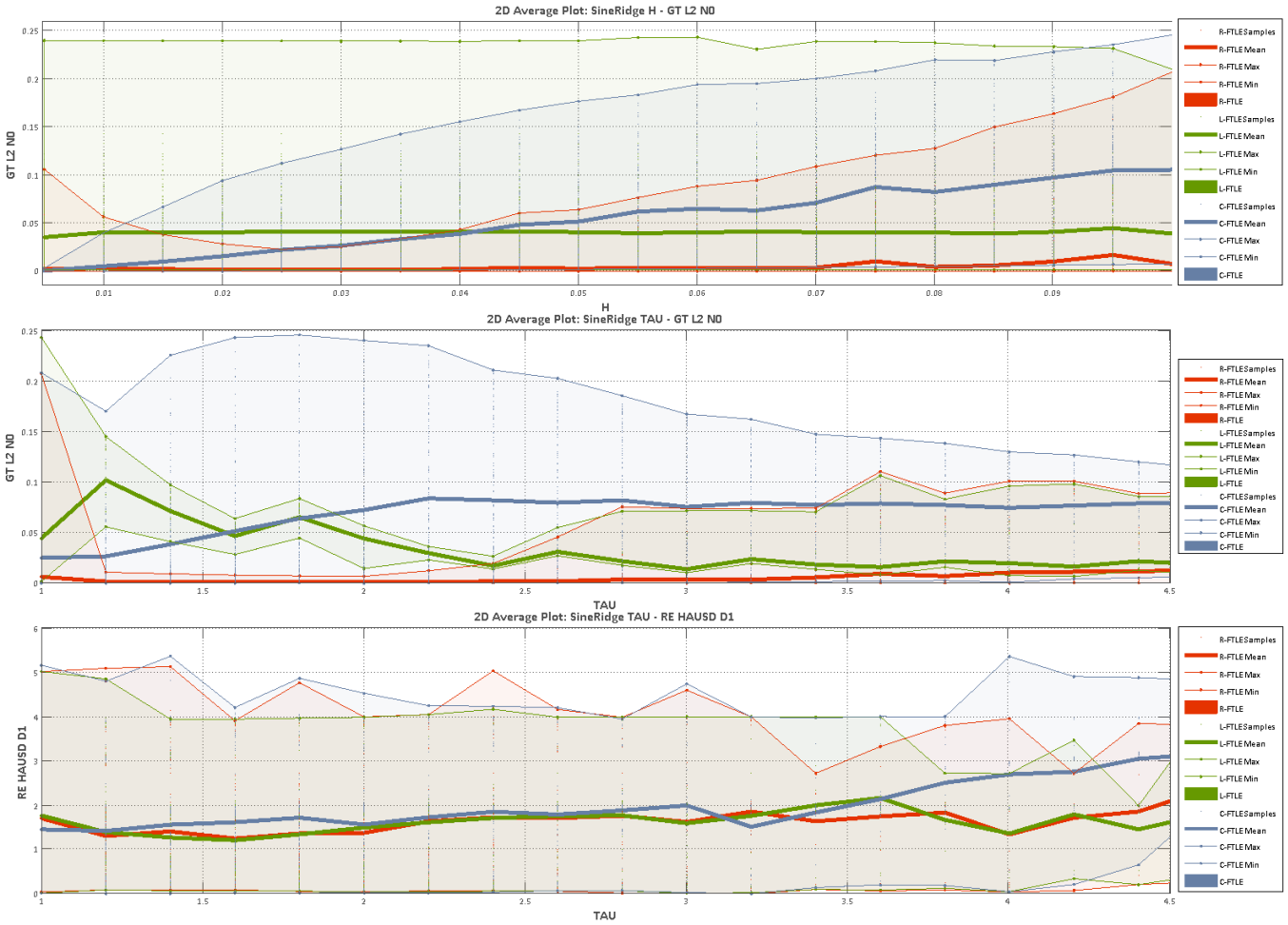


Figure 8: **Sine ridge:** Averaged curves of the sine ridge example for both error measures among all samples. Note, that *smaller* relative resolution $H$ values denote higher sampling densities.

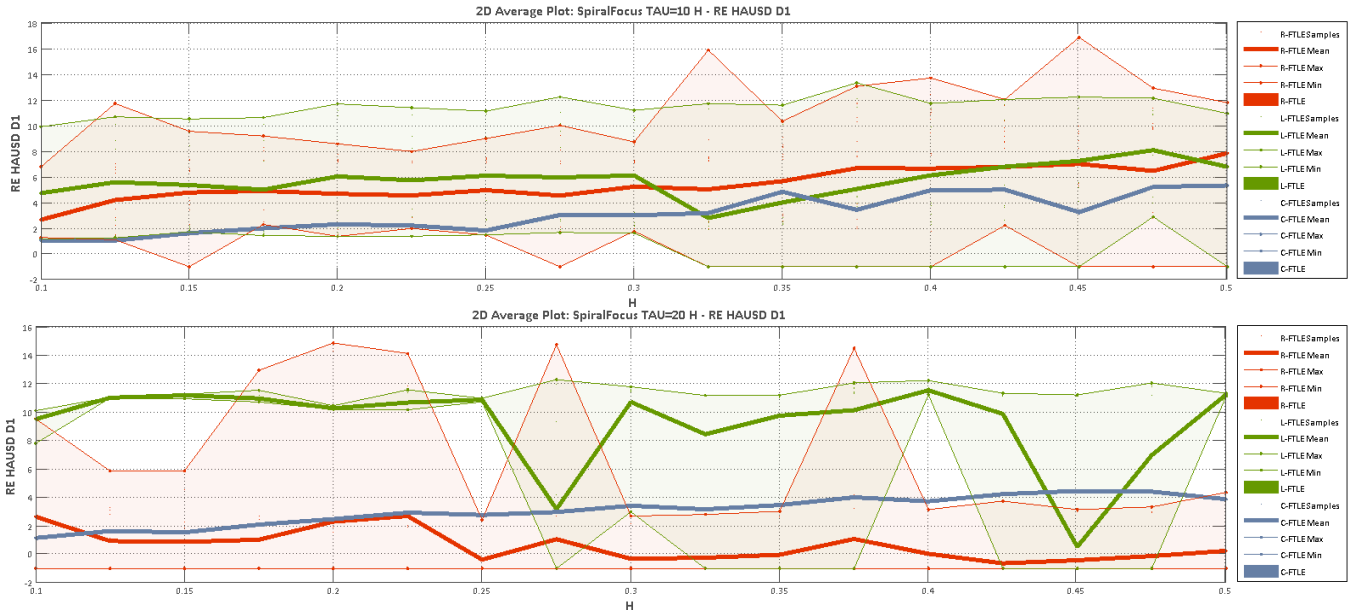


Figure 9: **Spiral focus:** If we compare all three methods regarding their behavior on increasing resolution, C-FTLE shows increasing performance for the ridge measure. L-FTLE especially produces worse results for long integration times, due to complex derivatives of the spiral focus example.

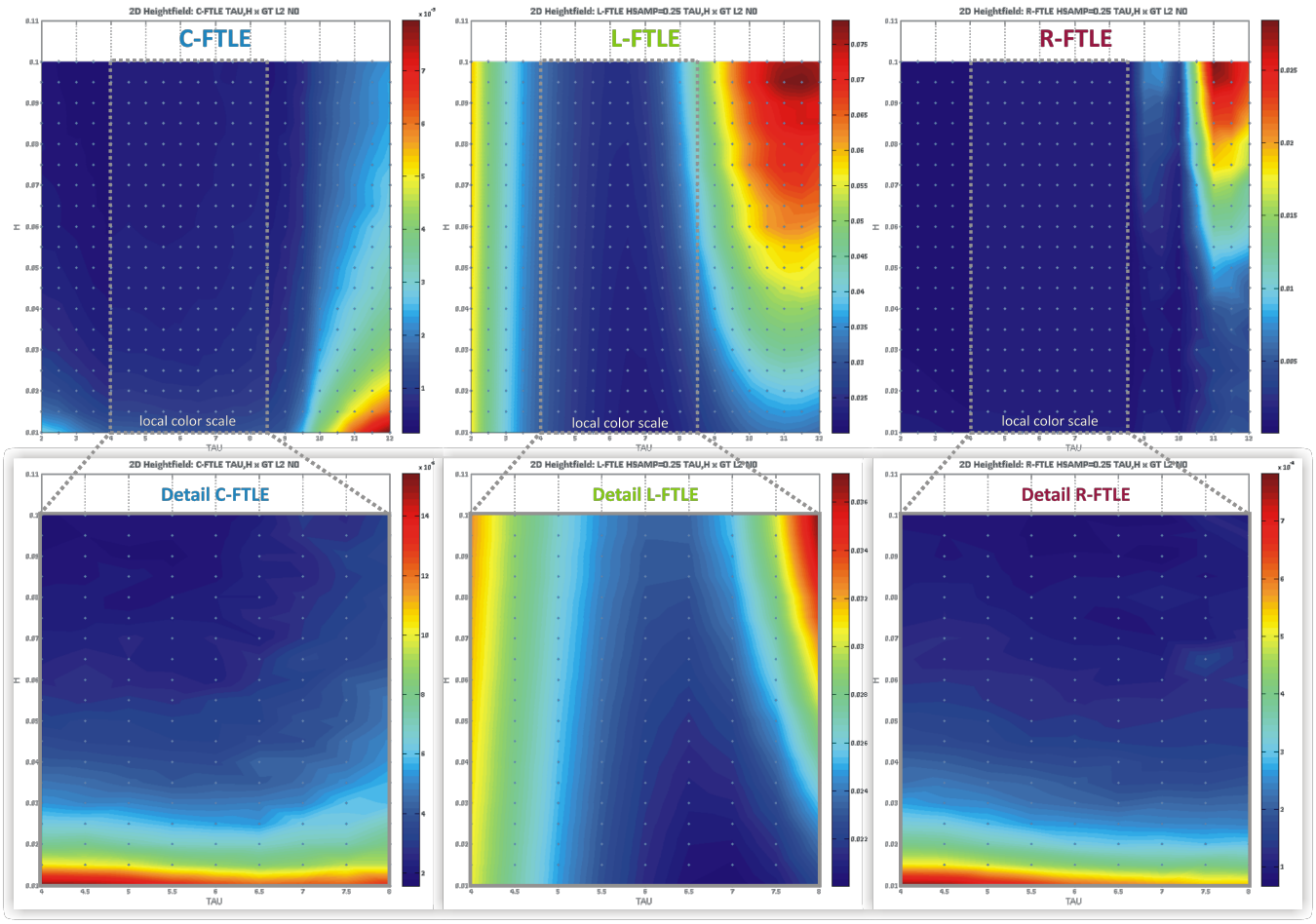


Figure 10: **Double gyre deformed:** Plots for the field error in *local* color scale. The top picture shows the resulting field error in dependence of resolution and integration time. Note, that for R-FTLE and L-FTLE the initial sampling distance $HSAMP$ has been fixed to $0.25$ in order to acquire an unique height surface.

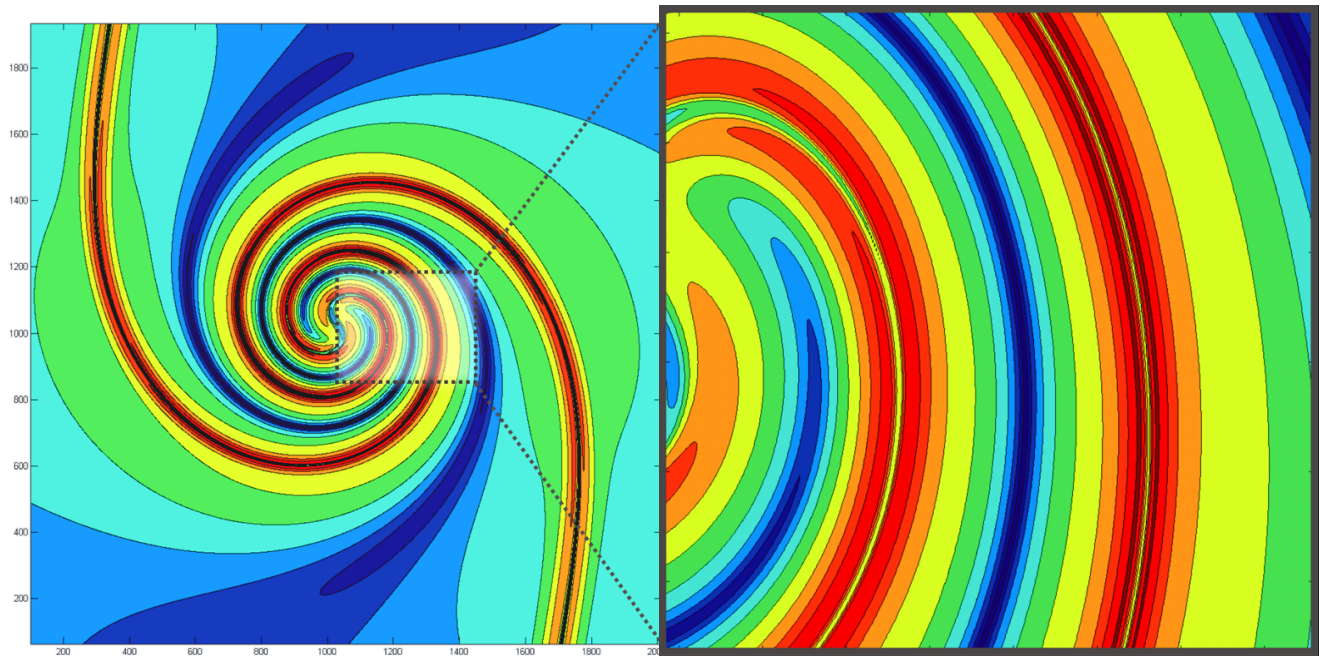

Figure 11: **Spiral focus:** Isocontour view of the FTLE field evaluated using the numerical ground truth for $P0 = 10$ showing the complexity and high detail of the resulting ridge structures.

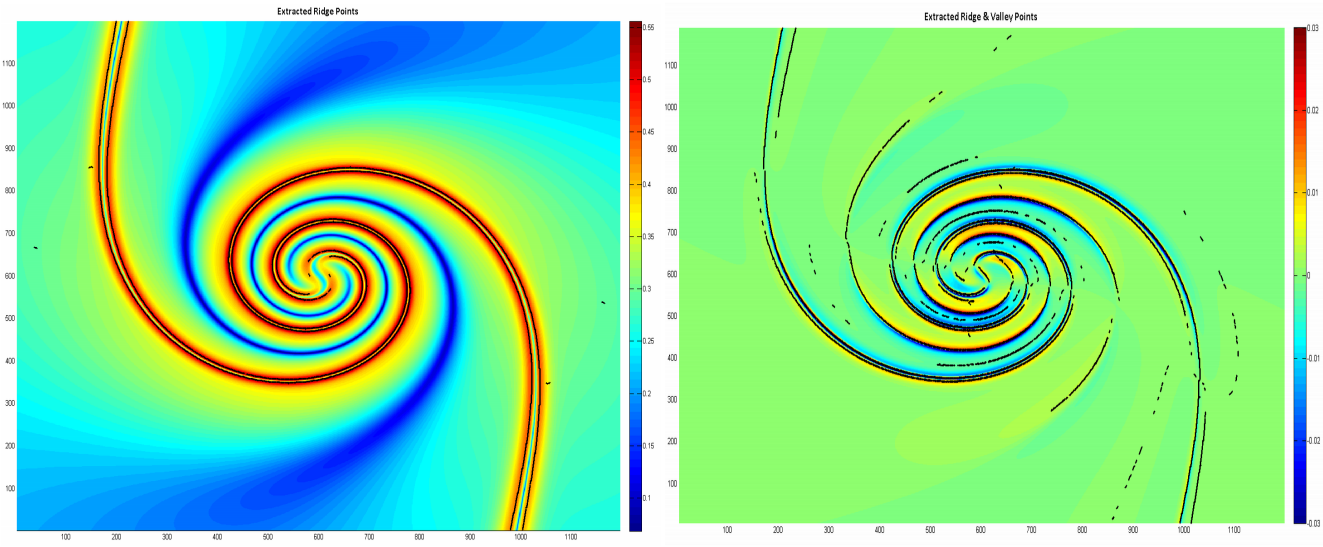


Figure 12: **Spiral focus**: This image illustrates the difference of two different ridge extraction methodologies. The left image shows an image based extraction similar to C-Ridges as presented by Schindler et al. [2] which works directly on the FTLE field. The right image shows the ridge extractor results for the definition of Eberly et al. [1]. The latter method delivers more cluttered results, as it also uses approximations of the 2nd derivatives (color coded in background). Note that we used explicitly the last method in order to reflect this aspect in our study. Without filtering, artifacts appear during extraction in both methods, depending on the parameter settings of the extractor.